Fuel Processing Technology 107 (2013) 126–137

Contents lists available at SciVerse ScienceDirect

Fuel Processing Technology

journal homepage: www.elsevier.com/locate/fuproc

Numerical simulation of a reversed flow small-scale combustor

M. Graça [a], A. Duarte [a,b], P.J. Coelho [a,*], M. Costa [a]

[a] Mechanical Engineering Department, Instituto Superior Técnico/IDMEC, Technical University of Lisbon, Avenida Rovisco Pais, 1049-001 Lisbon, Portugal
[b] Mechanical Engineering Department, Faculdade de Ciências e Tecnologia, Universidade Nova de Lisboa, 2829-516 Caparica, Portugal

ARTICLE INFO

Article history:
Received 28 March 2012
Received in revised form 14 June 2012
Accepted 25 June 2012
Available online 24 July 2012

Keywords:
Reversed flow combustor
Combustion models
Kinetic mechanisms
Eddy dissipation concept
Composition joint pdf

ABSTRACT

A numerical study of a reversed flow small-scale combustor is reported. The combustion chamber is a closed end cylinder with the burner and the exhaust port mounted at the top of the combustor. Natural gas was used as a fuel and the combustion air was preheated to 600 K. Two distinct conditions, achieved by varying the air flow rate were analyzed, the first being a conventional lean combustion regime and the second corresponding to the flameless combustion regime. The numerical simulations were carried out using ANSYS Fluent 13.0. Turbulence was modeled using the realizable k–ε model. The performance of two different combustion models, namely the eddy dissipation concept (EDC) and the composition PDF (C-PDF) model, was compared. Detailed chemical mechanisms for natural gas were employed. The sensitivity of the results to the mesh size, number of stochastic particles in the C-PDF model, reaction mechanism and constants of the models was investigated. A good agreement between the predictions obtained using the EDC and the C-PDF model was found. However, both models underpredict the measured temperature in the vicinity of the centreline in the region close to the burner, i.e., combustion is delayed in comparison with the experimental data, for both operating conditions.

1. Introduction

In the past few decades, increasing environmental concerns with pollutant emissions from conventional combustion sources and awareness of limited fossil fuel resources have led to the development of advanced techniques aiming at a reduction of pollutant emissions, while maintaining or improving the overall thermal efficiency of combustion systems. Emissions of nitrogen oxides (globally referred to as NO_x), responsible for the formation of atmospheric smog and acid rains, have been reduced using several different techniques, such as exhaust gas recirculation, reburning and staged combustion. In the early 1990s, a new combustion regime called Flameless oxidation (FLOX), also referred to in the literature as MILD (Moderate or Intense Low Oxygen Dilution) combustion, HiTAC (High Temperature Air Combustion), or CDC (Colourless Distributed Combustion), was identified [1]. Since then, it has been widely investigated, both experimentally and computationally, as a new promising way to reduce pollutant emissions and achieve high thermal efficiency [2].

Extensive work has been carried out to investigate the conditions required to operate in the flameless oxidation regime, and to understand the underlying physical mechanisms, as well as to demonstrate the advantages that it presents in comparison with other combustion systems and emissions reduction technologies. This regime is characterized by lower mean temperatures and turbulent temperature fluctuations, low NO_x emissions, and a nearly invisible and inaudible flame. The lower temperature is achieved by highly diluting the combustion air with flue gas, providing not only heat for ignition, but also increasing the specific heat capacity of the reactive mixture, which contributes to the reduction of the temperature. Therefore, the formation of thermal NO via the Zeldovich mechanism [3] is inhibited, or at least greatly reduced. By combining the dilution with air preheating (which would, by itself, increase the overall efficiency while greatly increasing emissions), a clean and efficient combustion regime is attained. As a consequence of the attractive features of flameless combustion outlined above, this combustion regime has been successfully applied to various industrial furnaces [4], and its potential application to gas turbine combustors has been investigated [5,6].

Considering the importance of achieving sufficiently high levels of oxygen dilution with flue gas in order to obtain the desired reduction of NO_x emissions, the combustion chamber geometry is of obvious importance. Multiple studies have been made with different geometries and various burner arrangements with this goal in mind. Pioneering research work was simultaneously carried out in Japan, Germany and at the International Flame Research Foundation (IFRF), in The Netherlands. Nakamachi et al. [7] patented a burner with two fuel injectors positioned away from the central stream of hot preheated combustion air. Wünning and Wünning [1] designed a combustor with a central natural gas jet surrounded by jets of

* Corresponding author. Tel.: +351 218418194.
E-mail address: pedro.coelho@ist.utl.pt (P.J. Coelho).

0378-3820/$ – see front matter © 2012 Elsevier B.V. All rights reserved.
doi:10.1016/j.fuproc.2012.06.028

preheated air. A burner with a central gas injector and individual air injectors located in a circumference around the gas injector was developed at IFRF [8]. Many other burner and combustor configurations have been investigated since then (see, e.g., refs. [9–13]).

The design of the present combustor geometry is somewhat similar to that investigated by Plessing et al. [14], in which the burner and the exhaust are placed at the same side of the combustor, the opposite side being closed. Plessing et al. [14] employed optical methods to visualize the reaction zone and to identify the burning and mixing regions. They concluded that the reaction zone was distributed throughout the volume of the chamber and the temperature distribution was considerably more uniform than in conventional combustion regimes. Moreover, the results suggested that the time scales associated with chemical reactions were larger than those associated with turbulent mixing. Further experimental work by Özdemir and Peters [15] in the same combustor provided an extensive characterization of the flow aerodynamics inside the chamber using laser Doppler velocimetry and concluded that the previous observation concerning the time scales is a consequence of the high level of reactants dilution with flue gases. These observations have important consequences in the mathematical modeling of this combustion regime. In fact, the temperature and species concentration gradients are smoother than in conventional flames and the combustion model should be able to predict reactive flows with low Damköhler numbers, in which combustion may be controlled by kinetics, in contrast to conventional diffusion flames, which are generally controlled by mixing. Coelho and Peters [16] employed an in house CFD code as well as the commercial Fluent code with the Eulerian particle flamelet model to predict the reactive flow in the combustor studied by Plessing et al. [14]. Good agreement with the experiments was found for the velocity field predictions in both codes, but the experimental validation was limited. Dally et al. [17] studied the effect of fuel type on the stability and characteristics of the flames, and on the establishment of MILD combustion in the same furnace. Szegö et al. [18,19] designed and studied experimentally a MILD combustor with a square cross-section, closed on the top, and the burner and the exhaust located at the bottom. The combustor has a single air nozzle, located at the center of the bottom wall, and four exhaust and four fuel ports arranged symmetrically in a ring pattern on the same wall.

It is interesting to point out that a few older works studied reverse flow combustor configurations [20,21], but they do not report any evidence of flameless combustion. More recently, several researchers investigated a stagnation point reversed flow combustor that operates stably with very lean fuel–air mixtures, and in both premixed and non-premixed modes, with low emissions [22–24]. However, according to their simulations, the flow times are too short for auto-ignition at the operating equivalence ratio so that the combustor does not appear to operate in flameless mode [22].

The aim of the present work is to report numerical simulations of the reverse flow small-scale combustor experimentally studied by Castela et al. [25]. The burner consists of a central fuel jet and an annular air inlet, and the exhaust is through a concentric annular ring. Both the burner and the exhaust are located at the top of the combustor, and the bottom section is closed. This arrangement leads to a self-reversing flow, which enhances the entrainment of the flue gas and fresh reactants, therefore enhancing the oxygen dilution, which is a precondition for flameless combustion. Furthermore, the increased residence time in the recirculation zone has the effect of improving flame stability with higher reactant velocities.

Accurate numerical simulation of combustors operating in the flameless regime is a challenging task. A survey of the literature shows that a significant number of studies have been reported, using a wide variety of turbulence and combustion models. However, the validation is generally scarce, since there is not much detailed experimental data available. Moreover, many studies show difficulties in the prediction of the near burner region. As far as the turbulence model is concerned, comparisons reported in the literature using the standard, RNG and realizable k–ε models and the Reynolds stress model show only minor differences [26–29]. In contrast, the combustion model has a greater influence on the predictions. In fact, several combustion models rely on the assumption of fast chemistry, which does not hold in the flameless regime. Hence, significantly different performance has been found in the modeling of combustors operating in the flameless regime, depending on the combustion model employed. In general, predictions obtained using the eddy dissipation concept, EDC [30], are satisfactory, even though validation is often limited, as mentioned above. Therefore, many studies have been reported using this model [28,31–37]. In addition, several works have used the EDC to simulate a jet in a hot diluted co-flow that emulates the MILD combustion regime [38–44]. One of the most advanced combustion models is the joint composition pdf transport model [45]. This model has not been applied to the simulation of combustors operating in the flameless regime, even though it was applied to the modeling of a jet in a hot diluted coflow [46]. The present work reports a comparison of the EDC with the joint composition pdf transport model for a reverse flow small scale combustor using the comprehensive experimental data of Castela et al. [25].

2. Experimental

Fig. 1 shows a schematic of the combustor modeled in this study. The combustion chamber is a quartz-glass cylinder with an inner diameter of 100 mm and a length of 340 mm. During the tests, the quartz cylinder was insulated with a 30-mm-thick ceramic fibre blanket. The burner and the exhaust port are mounted at the top end of the combustion chamber. The burner consists of a central orifice of 4 mm inner diameter, through which the fuel is supplied, surrounded by an annular orifice with 14 mm inner diameter and 18.5 mm outer diameter for the combustion air supply. The exhaust consists of an annular orifice, concentric with the burner, with 75 mm inner diameter and 90 mm outer diameter. A stainless steel plate is used to close the bottom end of the combustion chamber. This plate contains a moving hole with an inner diameter of 11 mm that allows for the introduction of probes. The combustion air is preheated by an electrical heating system that allows air inlet

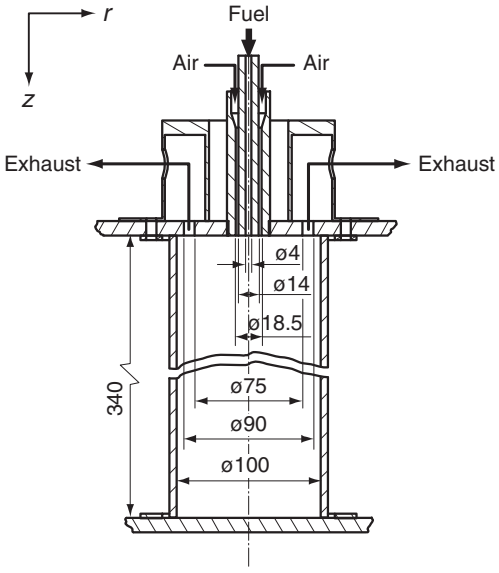

Fig. 1. Schematic of the combustor.

temperatures up to 980 K, which are monitored by a type K thermocouple installed at the entrance of the burner.

The experimental data are reported and discussed in ref. [25]. Local mean temperature measurements were obtained using 76 μm diameter fine wire platinum/platinum: 13% rhodium (type R) thermocouples. The uncertainty due to radiation heat transfer was estimated to be less than 5% by considering the heat transfer by convection and radiation between the thermocouple bead and the surroundings. The sampling of the gases for the measurement of local mean major species concentrations was achieved using a stainless steel water-cooled probe. The analytical instrumentation included a magnetic pressure analyzer for O_2 measurements and a non dispersive infrared gas analyzer for CO_2 and CO measurements. Quenching of the chemical reactions was rapidly achieved upon the samples being drawn into the central tube of the probe due to the high water cooling rate in its surrounding annulus. No attempt was made to quantify the probe flow disturbances. On average, the repeatability of the gas species concentration data was within 10% of the mean reported value.

In this study, natural gas (CH_4: 83.7%, C_2H_6: 7.6%, C_3H_8: 1.9%, N_2: 5.4% and other components with minor concentrations) was used as fuel. Table 1 summarizes the test conditions used for the detailed in-combustor measurements. Run 1 corresponds to a conventional lean flame condition and run 2 corresponds to a flameless condition [25].

3. Mathematical model

The mathematical model is based on the numerical solution of the Favre-averaged governing equations for mass, momentum and energy and on transport equations related to the turbulence and combustion models. Turbulence was modeled using the realizable k–ε model [47], which involves the solution of transport equations for the turbulent kinetic energy and its dissipation rate. Two different combustion models were used, namely the EDC [30] and the joint composition pdf transport model [45].

The EDC is an improved version of the eddy dissipation model [48], which is able to use detailed finite-rate chemical kinetics in the simulation of turbulent reactive flows. Transport equations for the species are solved during the CFD calculations, so that the computational requirements are higher than those of models based on the conserved scalar formulation with a prescribed pdf shape, such as the laminar flamelet model, in which the chemistry is decoupled from the CFD calculations and tabulated. However, models based on this formulation rely on the fast chemistry assumption. The EDC is not restricted to fast chemistry flows, and is able to simulate both high and low Damköhler number flows.

The EDC relies on the Kolmogorov cascade of energy dissipation on all length scales in turbulent flows from the largest eddies to the smallest ones. It assumes that chemical reactions, as well as molecular mixing associated with turbulence dissipation, occur within the fine structures of the flow, defined as a small fraction of the total fluid volume where the reactants are homogenously mixed, similarly to a well stirred reactor. The velocity and length scales of these fine structures, denoted by u^* and L^*, respectively, are defined as a function of the dissipation rate of turbulent kinetic energy, ε, and the kinematic viscosity, ν:

$$u^* = 1.74\,(\varepsilon\nu)^{1/4} \tag{1}$$

$$L^* = 1.43\left(\nu^3/\varepsilon\right)^{1/4} \tag{2}$$

where the superscript * refers to the fine structures. Moreover, assuming that the fine structures are located in nearly constant energy regions, the mass fraction they occupy is given by:

$$\gamma^* = \gamma_\lambda\left(u^*/u'\right)^2 \tag{3}$$

where u' is the root mean square fluctuating velocity of the largest turbulent eddies. The mass fraction occupied by the fine structure regions, γ_λ, is given by:

$$\gamma_\lambda = u^*/u' \tag{4}$$

Inserting Eq. (1) in Eq. (4), and assuming that the turbulent kinetic energy, k, is given by $k=(1.5\,u'^2)^{0.5}$, the following expression is obtained:

$$\gamma_\lambda = C_\gamma\left(\nu\varepsilon/k^2\right)^{1/4} \tag{5}$$

where C_γ is a volume fraction constant whose value is 2.1377. The reactions are assumed to occur in the fine structures over a residence time scale τ^* defined as:

$$\tau^* = C_\tau(\nu/\varepsilon)^{1/2} \tag{6}$$

where C_τ is a time scale constant equal to 0.4082. The mean reaction rate in the conservation equation for the ith species, R_i, is modeled as:

$$R_i = \frac{\bar\rho\,\gamma_\lambda^2}{\tau^*\left(1-\gamma_\lambda^3\right)}\left(Y_i^* - \tilde Y_i\right) \tag{7}$$

In this equation, $\bar\rho$ is the mean fluid density, Y_i^* the mass fraction of species i within the fine structures after reacting over the time τ^*, and $\tilde Y_i$ is the Favre-averaged mass fraction of species i obtained from:

$$\tilde Y_i = \gamma_\lambda^3 Y_i^* + \left(1-\gamma_\lambda^3\right)Y_i^o \tag{8}$$

Here, Y_i^o represents the mass fraction of species i in the fluid surrounding the fine structures.

The composition joint pdf (C-PDF) method offers an alternative to study turbulent reacting flows through a stochastic method, allowing the influence of turbulent fluctuations on the mean chemical source term to be determined without any modeling assumptions. This model calculates the composition joint probability density function of the temperature and the mass fractions of the species. The mean values of the temperature and species mass fractions may be evaluated from the composition joint pdf, P, for all the species mass fractions and for the enthalpy of mixture.

The joint pdf transport equation may be written in the following form:

$$\frac{\partial\left(\bar\rho\,\tilde P\right)}{\partial t} + \frac{\partial\left(\bar\rho\,\tilde u_j\,\tilde P\right)}{\partial x_j} + \frac{\partial\left(\bar\rho\,S_i\,\tilde P\right)}{\partial\psi_i} = -\frac{\partial\left(\bar\rho\left\langle u''_j\middle|\psi\right\rangle\tilde P\right)}{\partial x_j} + \frac{\partial}{\partial\psi_i}\left(\bar\rho\left\langle\frac{1}{\bar\rho}\frac{\partial J_{ji}}{\partial x_j}\middle|\psi\right\rangle\tilde P\right) \tag{9}$$

Table 1
Test conditions for the detailed in-combustor measurements[a].

Run	Excess air coefficient (λ)	Air inlet velocity (m/s)	Flue-gas (ppm @ 15%O_2)	
			CO	NO_x
1	1.5	66	1	23
2	2.4	108	1	1

[a] For all conditions: atmospheric pressure; fuel thermal input = 8 kW, fuel inlet velocity = 17.7 m/s; air inlet temperature = 600 K; fuel inlet temperature = 300 K.

where the tilde denotes a Favre-average value, the double prime a fluctuation about a Favre-average value, the angle brackets a probabilistic mean, or expected value, and the symbol $<A|B>$ represents the conditional probability of A, given that B occurs. The symbol t is the time, x_j the spatial coordinate in j direction, ψ_i the ith component of the composition vector, u_j the velocity component in j direction, S_i the source term for the ith component of the composition vector, ψ the composition space variable and $J_{j,i}$ the molecular diffusion flux of the ith component of the composition vector in j direction. The first two terms on the left side of this equation represent the rate of change and advection of the pdf in the mean flow, and the third one describes the transport of the pdf in composition space by chemical reactions. These three terms are in closed form, i.e., they do not need modeling. In contrast, the two terms on the right-hand side require modeling. The first one accounts for the transport in physical space due to turbulent convection, and is modeled using the gradient diffusion assumption as follows:

$$-\frac{\partial\left(\bar{\rho}\left\langle u''_j\middle|\psi\right\rangle\tilde{P}\right)}{\partial x_j}=\frac{\partial}{\partial x_j}\left(\frac{\bar{\rho}\mu_t}{Sc_t}\frac{\partial\tilde{P}}{\partial x_j}\right) \tag{10}$$

where μ_t is the turbulent viscosity and Sc_t the turbulent Schmidt number. The last term on the right side of Eq. (9) represents the transport in scalar space due to molecular mixing. This term was modeled using the Euclidean Minimum Spanning Tree (EMST) [49]. This mixing model takes into account the physical position of the particles to be mixed, and is the most accurate mixing model available in the CFD code used in this work.

The joint pdf transport equation was solved using the Monte Carlo method. Notional particles with mass move randomly through the physical space, due to particle convection, and through the composition space, due to molecular mixing and chemical reactions, in fractional time steps, allowing the position, the temperature and the mass of the particles to be found after every time step. The temperature and the mass fraction of the particles present in a given control volume are averaged to yield the mean temperature and the mean mass fraction of the species in that control volume.

The DRM19 chemical mechanism [50] was used in this work to describe the combustion of natural gas, while the GRI-Mech 1.2 mechanism [51] and a global methane-air reaction mechanism [52] were also used for comparison purposes. We have performed further calculations using the GRI-Mech 2.11 mechanism [51], comprising 49 species, but they are not reported here, since the predictions were found to be very similar to those obtained using the GRI-Mech 1.2 mechanism. The GRI-Mech 1.2 mechanism comprises 32 species and 177 reactions. The DRM19 mechanism is a subset of the GRI-Mech 1.2 full mechanism, with 19 species and 84 reactions, developed to obtain the smallest set of reactions needed to closely reproduce the main combustion characteristics predicted by the full mechanism. Since the computational time of the C-PDF model is very sensitive to the number of species in the chemical mechanism, this model was only used along with the DRM19. In the case of the EDC, both the DRM19 and the GRI-Mech 1.2 mechanisms were used to check whether the reduced mechanism reproduces or not predictions of the detailed mechanism.

The in-situ adaptive tabulation (ISAT) method [53] was used to reduce the computational cost for both the EDC and the C-PDF methods. The default ISAT tolerance (10^{-3}) was used until a moderately converged solution was obtained, and a smaller tolerance (10^{-4}) was set thereafter.

Thermal radiation was taken into account using the discrete ordinates method and the radiative properties of the participating medium were modeled by the weighted-sum-of-grey gases model, in which the spatial variation of the total emissivity is computed as a function of the H_2O and CO_2 local mass fractions and temperature.

The calculations were performed using ANSYS Fluent 13.0. Uniform axial velocity profiles of air and fuel were prescribed at the inlet section of the admission ducts, which are included in the computational domain in order to allow the flow to develop prior to the entrance at the combustion chamber. The turbulent kinetic energy and dissipation rate were prescribed using the method suggested by Versteeg and Malalasekera [54]. Standard wall functions were used for the velocity boundary conditions at the walls of the combustor. The wall temperature was set to 1300 K, based on experimental measurements, and the emissivity was set to 0.9. Pressure outlet with zero gauge pressure was used for the boundary condition at the exhaust. All the governing equations were solved using a second order upwind discretization scheme, and a coupled solver was used. The convergence criterion demanded that the sum of the residuals of the discretized equations over the domain dropped below 10^{-3}, except for energy, where a tolerance of 10^{-6} was used. In addition, it was requested that the values of certain key properties, namely the mean temperature and mean mass fraction of major species, in several monitoring points of the computational domain, become approximately constant during the course of the iterative solution process. It was found that this second criterion was more demanding, i.e., it was necessary to continue the iterative process after the first criterion was satisfied, until the variations of the monitored values became negligible, which corresponded to a decrease of the residuals up to about 10^{-5}.

4. Results and discussion

Predictions of the temperature and species molar fraction fields in the reverse flow combustor are presented in this section and compared with the experimental data of Castela et al. [25] for the two runs identified in Table 1, corresponding to different excess air coefficients. According to their analysis, the first run corresponds to conventional lean combustion, while the second one achieves the flameless oxidation regime. For both runs, predictions performed using both the EDC and the C-PDF combustion models are shown, using the DRM19 chemical mechanism. Further predictions are presented using modified values of constants of the turbulence and combustion models, as well as different chemical mechanisms, in order to ascertain the influence of these changes on the temperature and species concentration. The results for run 1 are presented in sections A to E, while those for run 2 are reported in section F.

4.1. Grid convergence study

The computational domain was mapped using two different 2D-axisymmetric meshes with approximately 14,000 and 50,000 control volumes. The fuel and air ducts are included in the computational domain, in order to reduce the uncertainty on the definition of the boundary conditions for the turbulent kinetic energy and dissipation rate at the entrance to the combustor. The grids are structured, with rectangular control volumes, and non-uniform, being more refined in the near burner region and mixing zones, in order to accurately calculate the velocity field and the temperature and species concentration gradients in these regions.

A comparison between the predictions obtained for the meshes using the EDC is shown in Fig. 2. Radial profiles of temperature and molar fractions of CO_2 and O_2 are shown at two different sections, $z=70$ mm and $z=150$ mm, representative of the behavior found elsewhere. The origin $z=0$ mm is located at the top of the quartz cylinder, i.e., at the exit of the fuel and combustion air ducts. Temperature differences between the two meshes are marginal. The O_2 molar fraction differences are also negligible, while differences in the CO_2 molar fraction are relatively small, and do not exceed 0.005. The velocity field, not shown in this figure, was also similar for the two

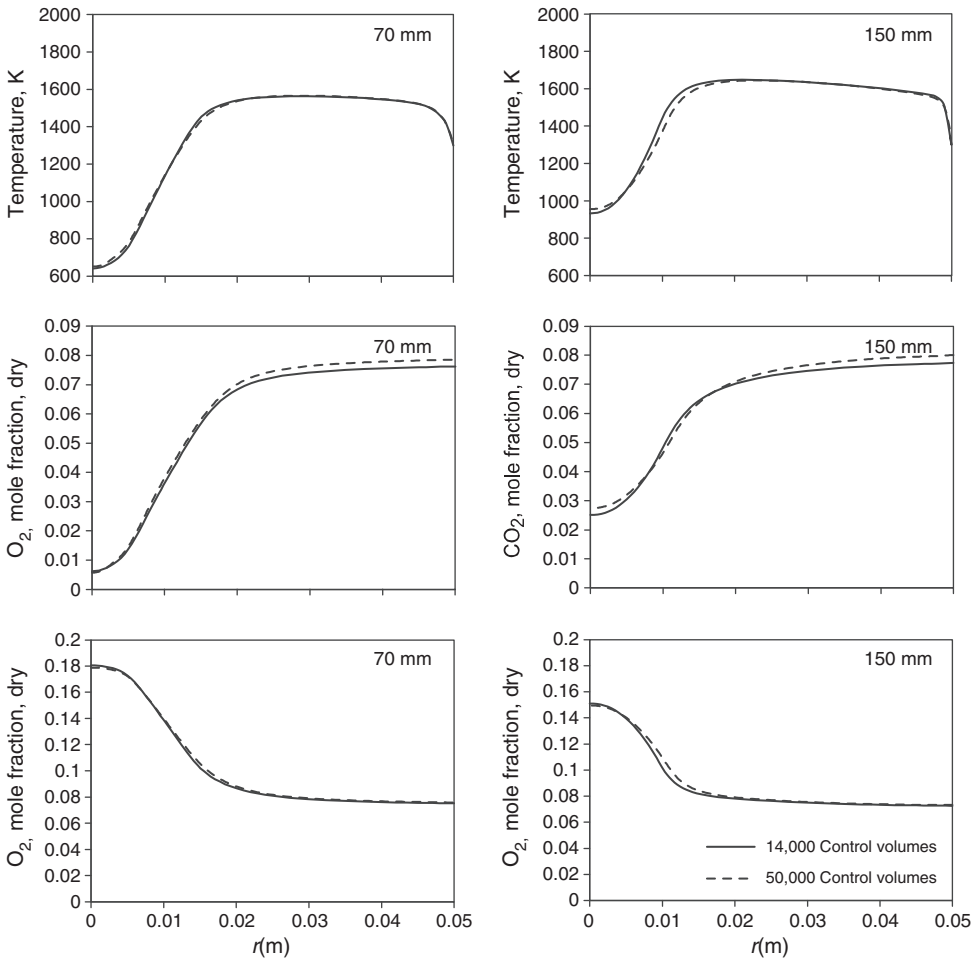

Fig. 2. Influence of the grid size on the predictions of the EDC model.

meshes. Hence, the coarsest grid was selected to perform the simulations reported in the remainder of this paper.

An analysis of the influence of the number of stochastic particles per control volume in the C-PDF method was also carried out. This sensitivity study was performed using a single-step global reaction mechanism, in order to save CPU time. The results are plotted in Fig. 3 and show that 150 particles per control volume yield predicted molar fractions of CO_2 and O_2 that are rather similar to those calculated by doubling the number of particles. In contrast, significantly different results are obtained using 60 particles per control volume. The temperature profiles still show differences up to 50 K when the number of particles is increased from 150 to 300. The calculations presented below were performed using 250 particles per control volume, in order to minimize the influence of the grid on the temperature field and save CPU time. The mean axial velocity profiles, not shown here, exhibit a negligible dependence on the number of particles for the tested values.

4.2. Flow pattern

The predicted flow pattern using the C-PDF and the DRM19 chemical mechanism is shown in Fig. 4. At present there are no measurements of the velocity field within the combustor. Fig. 4 shows that the closed bottom of the combustion chamber promotes a long recirculation zone that extends over a large part of the combustor. However, the velocities are quite small near the closed bottom, where a quasi-stagnant region is present. The recirculated hot combustion products transport momentum and energy to the top of the combustor. The hot temperature of the walls of the combustor contributes to achieve relatively high and uniform temperature and species concentration of the recirculated products, which either leave the combustor through the exhaust, or mix with the incoming combustion air jet. The high momentum of the air jet creates a recirculation zone downstream of the fuel nozzle. A fraction of the combustion air entering the combustor entrains the recirculation zone and mixes with the fuel, whose momentum is relatively low. Hence, the fuel is engulfed by the recirculated air and rapidly mixes with the high momentum air jet entering the combustor.

4.3. Comparison between the EDC and the C-PDF models

Predicted radial profiles of temperature and molar fractions of CO_2, O_2 and CO obtained using the EDC and the C-PDF models for run 1 are presented in Fig. 5 along with experimental data. Significant discrepancies can be seen in the first two profiles at $z = 70$ mm and $z = 150$ mm. The experimental data show that the temperature in the vicinity of the centreline is quite high and that the molar fraction of CO_2 is significant and increases between the two stations, while the O_2 molar fraction has an opposite behavior. This means that combustion is taking place, and most of the fuel is burnt at $z =$ 150 mm. In contrast, the temperatures predicted by both models are low at $z = 70$ mm, as well as the CO_2 molar fraction. There is an

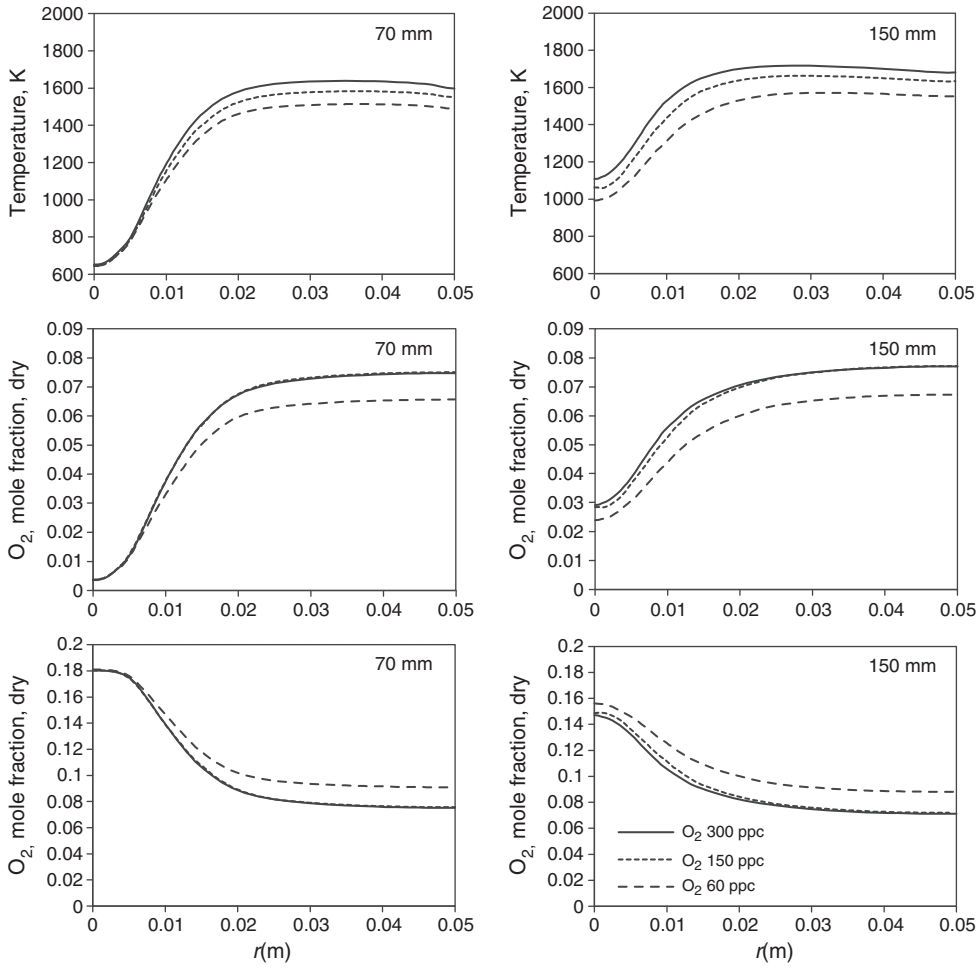

Fig. 3. Influence of the number of particles per control volume on the predictions of the C-PDF model.

increase between the two stations, but both quantities remain well below the experimental data at $z = 150$ mm. The O_2 molar fraction exhibits an opposite behavior, as expected. Therefore, both models predict a combustion process occurring further downstream. In the last station shown in Fig. 5, as well as in the region of the recirculated combustion products, the predictions from both combustion models are in much closer agreement with the experimental data. Predictions of the CO molar fraction show also significant shortcomings.

In an attempt to explain the discrepancies outlined above, additional calculations were carried out using the EDC model along with different turbulence models, namely the standard and the RNG variants of the k–ε model, and also the Reynolds stress model. These results are not shown here, since they reveal that the influence of the turbulence model is rather small in comparison with the discrepancies shown in Fig. 5. The influence of the boundary conditions for the turbulent kinetic energy and its dissipation rate was also studied, but it was found to be negligible for this combustor and these operating conditions. It is also likely that the fuel temperature at the nozzle exit, which was considered equal to the ambient temperature in the numerical simulations, is a little higher in the experiments due to heat transfer from the annulus with hot air surrounding the fuel pipe to the fuel. In order to investigate the influence of this effect on the results, additional calculations were carried out using an inlet fuel temperature of 400 K. It was found that the differences between the original results and the new ones are negligible, so that this effect does not explain the discrepancies between measured and computed mean temperature profiles in the near burner region.

Further insight into the predictions is provided by Fig. 6, which shows the ratio of the reaction rate due to chemical kinetics to the reaction rate due to turbulent mixing calculated using the eddy dissipation/finite rate model with a global single-step reaction. Although the quantitative values should be regarded with some care, due to the simplicity of this model, the results clearly reveal that, according to the predictions, the reaction rate due to chemical reaction is much lower than the reaction rate due to turbulent mixing in the burner region up to $z = 150$–200 mm. This yields a Damköhler number much lower than unity, in agreement with the predictions reported in Fig. 5, which show that chemical reactions are slow and only a small conversion of fuel into combustion products occurs in that region. Further downstream, the Damköhler number becomes greater than unity and combustion progresses rapidly, so that the predictions are in satisfactory agreement with the experimental data at the two last stations.

4.4. Comparison between reaction mechanisms

The influence of the chemical mechanism on the predictions for run 1 was investigated using both the EDC and C-PDF models. Three different mechanisms were studied, namely the DRM19 mechanism, the GRI-Mech 1.2 mechanism, and a global one-step reaction mechanism for methane and air. The DRM19 is a reduced reaction set based on the GRI-Mech 1.2. This last mechanism was not used together with the C-PDF model, because the computational time would be too long. The purpose of the comparison of reaction mechanisms reported in this section is to find out whether it is worth to rely on the more

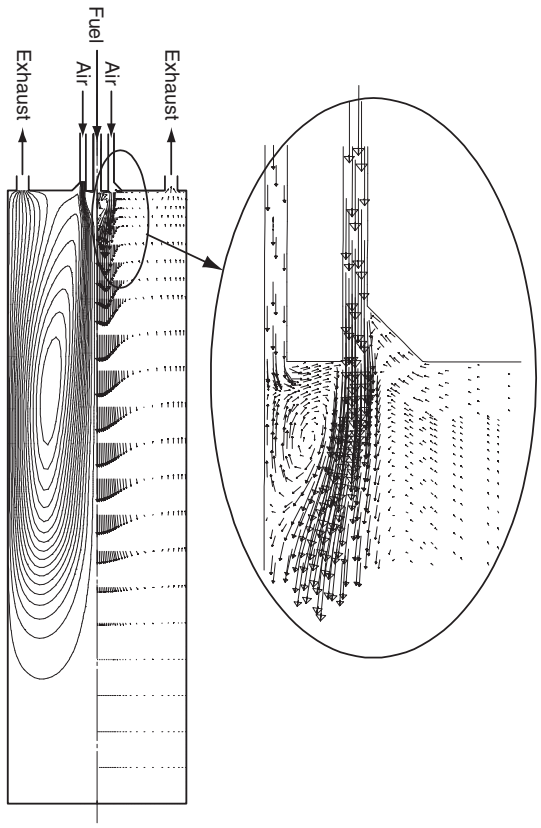

Fig. 4. Predicted flow pattern for run 1.

complex GRI-Mech 1.2 instead of the reduced version DRM19 or not, and to investigate how a global one-step reaction mechanism performs.

The results are displayed in Fig. 7. The predictions obtained using the EDC and the DRM19 are hardly distinguishable from those determined using the EDC and the GRI-Mech 1.2, as expected from the fact that the DRM19 is a reduced mechanism based on the GRI-Mech 1.2, but still relatively detailed. If the global one-step mechanism is used along with the EDC, combustion is even more delayed than for the detailed mechanisms. In fact, in the vicinity of the centreline, at $z =$ 204 mm, the temperature and the CO_2 molar fraction are lower and the O_2 molar fraction is higher than for the other mechanisms. The differences between the results calculated using the DRM19 and the global mechanism are much lower when the C-PDF model is employed instead of the EDC, even though the observed trend of a delayed reaction predicted by the global model is still visible. Hence, it can be concluded that the DRM19 is satisfactory for the present simulations, and there is no need to use the GRI-Mech 1.2. In contrast, the global mechanism yields worse predictions in comparison with the DRM19, but major differences are confined to the region where the fuel is burning.

4.5. Tests using modified realizable k–ε and EDC model constants

The standard k–ε model is able to simulate with engineering accuracy a wide range of turbulent flows using a unique set of constants. However, it is well known that the model has several limitations, inherent to the assumptions used in its formulation, and that modifications of the constants have been reported for some particular flows. As an example, the standard k–ε model overpredicts the spreading rate of a round jet, and a modification of constant $C_{\varepsilon 1}$ in the

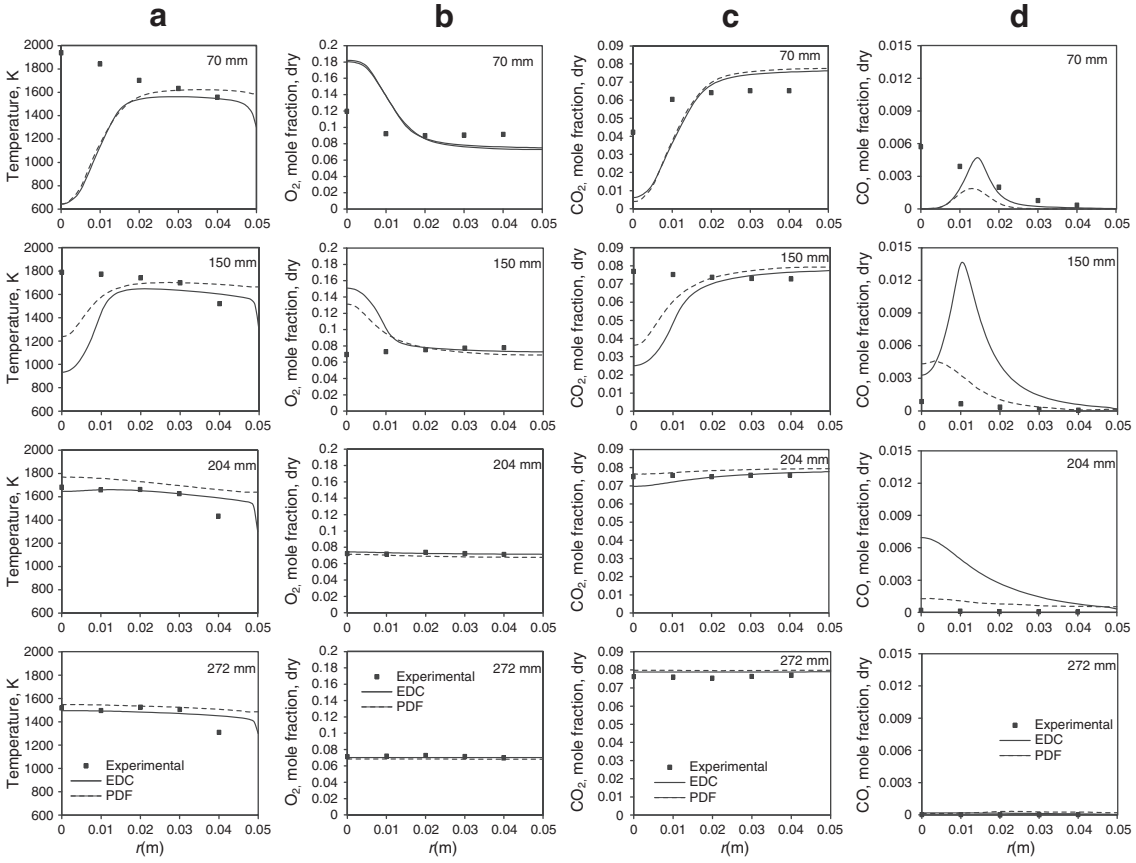

Fig. 5. Radial profiles of predicted temperature, O_2, CO_2 and CO dry mole fractions for run 1.

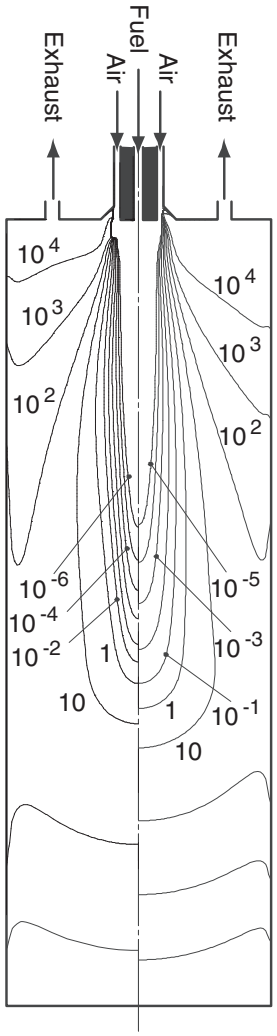

Fig. 6. Ratio of the reaction rate due to chemical kinetics to the reaction rate due to turbulent mixing calculated using the eddy dissipation/finite rate model (run 1 — left side, run 2 — right side).

transport equation for the dissipation rate of turbulent kinetic energy, ε, has been proposed to overcome this problem. However, the realizable version of the k–ε model, which uses a different transport equation for ε, successfully predicts the spreading rate of the round jet without any changes in the constants. Moreover, the flow configuration in the combustor under investigation is rather different from that of a round jet. In the present work, the sensitivity of the predictions to constant $C_{\varepsilon 2}$ was investigated (see Table 2). The effect of increasing the $C_{\varepsilon 2}$ constant of the realizable k–ε model is a decrease of the dissipation rate of turbulent kinetic energy, yielding increased spreading and decay rates for a turbulent reactant jet.

The constants C_τ and C_γ of the EDC model have been selected using data taken from several experiments, but these have not been clearly discussed, as pointed out by Aminian et al. [44], and therefore the range of validity of the values proposed for those constants is not so well established. The influence of these constants has been examined in a few recent works [42,44,55]. Rehm et al. [55] concluded that constant C_τ had almost no influence on the simulation of a high-pressure gasification process, but the mean reaction rate was strongly dependent on C_γ and the predictions could be improved by increasing the value of that constant. De et al. [42] simulated a jet in a hot coflow, and reported a too early ignition when the standard constants of the EDC model were used. However, they observed an improvement of the predictions when C_τ was increased from its default value to 3, and C_γ decreased to 1.0. Although, they managed to predict the location where ignition took place using the modified constants, they were not able to reach globally good results. They also claim that, for the standard value of C_γ, Eq. (7) is not valid if the turbulent Reynolds number, defined as $k^2/\nu\varepsilon$, is lower than 65. We have checked that, in our simulations, the Reynolds number exceeds this limit, except in the immediate vicinity of the walls. Recent simulations of a similar jet in hot coflow by Aminian et al. [44] support the conclusions of De et al. [42]. They argue that C_τ should be increased, and report improved results with that modification of C_τ. In the present work, the role of constant C_τ was found to be small, in contrast with the influence of C_γ. In fact, our predictions show a delayed rather than an early ignition, and therefore C_γ should be increased, as in the work of Rehm et al. [55].

The results obtained for the tests with the modified constants are shown in Fig. 8. This figure compares radial profiles of temperature and CO_2 molar fraction obtained using the default values of the constants with those of three simulations performed using modified constant values in accordance with Table 2. The effect of the modification of C_γ can be gleaned from an analysis of the gradient of the temperature and the CO_2 molar fraction in the reaction zone, resulting in a thinner and more intense reaction zone. A similar, but weaker, behavior results from the change of $C_{\varepsilon 2}$. Overall, a better agreement with the measurements is obtained by employing the modified values for $C_{\varepsilon 2}$ and C_γ constants, although the temperature and the CO_2 molar fraction are still significantly underpredicted at $z = 70$ mm and slightly underpredicted at $z = 150$ mm in the region close to the symmetry plane. It is worth to point out that even though the impact of the change of the constants may be anticipated, and despite the observed improvement obtained, there is no theoretical reason to justify either the new values of the constants or to expect similar performance in other reactive flows.

4.6. Predictions for flameless combustion

Fig. 9 shows the predicted temperature and molar fractions of CO_2, O_2 and CO for run 2. Overall, the quality of the predictions is similar for the two runs. In run 2 the measured temperature does not increase above ~1450 K and, as a consequence, the temperature levels within the combustor are lower than in run 1 and only marginally exceed 1400 K. The axial and radial temperature gradients are insignificant. The molar fractions of major species exhibit consistent trends, and reveal a slower conversion of reactants into products. The predictions reproduce this behavior, e.g., the predicted temperature in the vicinity of the centreline is lower in run 2 than in run 1. However, the discrepancies between the predictions and the experimental data remain significant downstream of the burner up to $z \approx 200$ mm. Elsewhere the predictions are relatively close to the measurements, except in the case of the CO molar fraction.

The results obtained using the C-PDF are slightly better than those calculated using the EDC. Even though both models predict a slower combustion process, the increase of mean temperature along the centreline is a little faster for the C-PDF, and the differences between the predicted and the measured species molar fractions of O_2 and CO_2 in the recirculated products are marginal for the C-PDF, in contrast with the EDC. The C-PDF predictions of CO are too low at $z \approx 70$ mm, and too high at $z \approx 200$ mm, as a consequence of the delayed combustion, but clearly more satisfactory than the EDC predictions.

The ratio of the reaction rate due to chemical kinetics to that due turbulent mixing, which was calculated using the eddy dissipation/finite rate model with a global single-step reaction, is shown in Fig. 6. The results are similar to those presented for run 1, i.e., the predicted rate of chemical reaction is much lower than the turbulent mixing rate in the burner region up to $z = 150-200$ mm. The increase of this ratio along the centreline is a little slower in run 2,

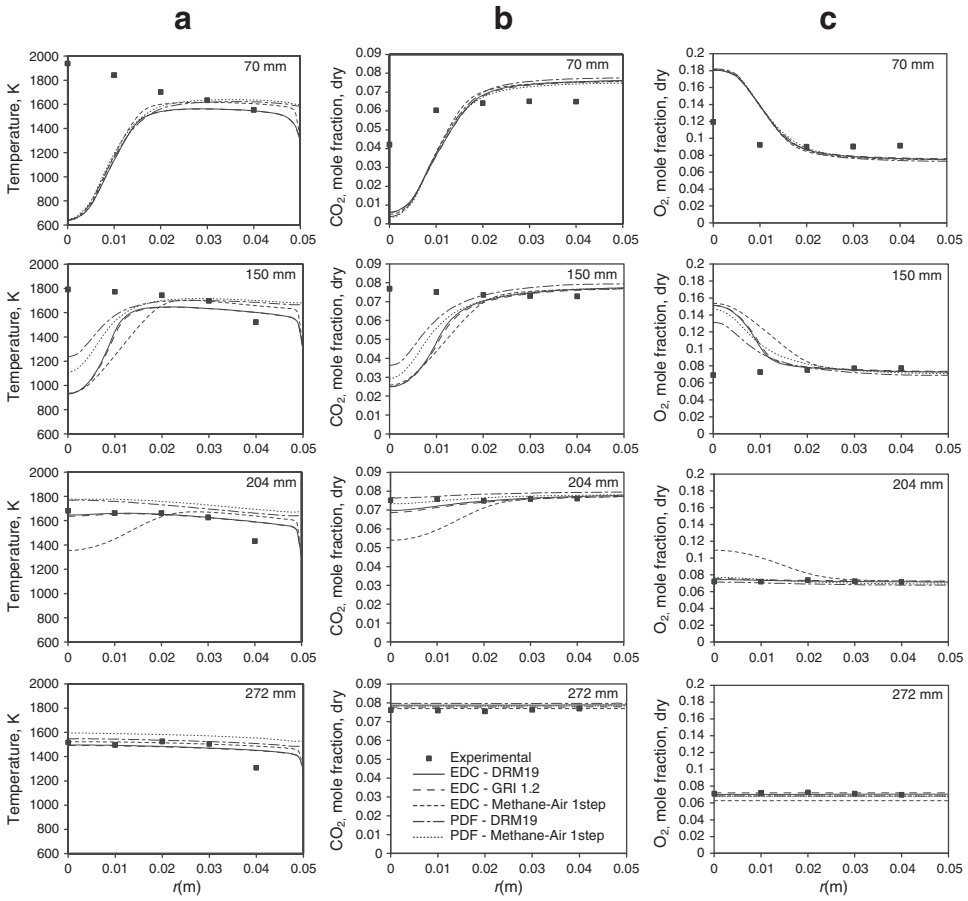

Fig. 7. Influence of the reaction mechanism on the predictions for run 1.

which is consistent with the predicted slower increase of temperature and CO_2 molar fraction. The similarity between the contours shown in Fig. 6 for runs 1 and 2, with Damköhler numbers lower than unity downstream of the burner, suggests kinetic controlled combustion processes, in agreement with the slow increase of the predicted temperatures along the centreline for both runs. In contrast, the measurements suggest different combustion processes for runs 1 and 2. In run 1, the very fast measured temperature rise downstream of the burner along the axial direction suggests a mixing controlled combustion process. In run 2, the uniformity of the temperature and molar fraction profiles is typical of a distributed reaction in the flameless regime.

The estimated recirculation rate, defined according to Wünning and Wünning [1], is 1.0, which is rather low compared with the values reported in the literature for flameless combustion (3 or more). This suggests that the predictions significantly underestimate the amount of recirculated exhaust gases, which may be the reason for the poor predictions observed downstream of the burner up to about one half of the length of the combustor. A strong underprediction of the entrainment has also been reported in ref. [27].

Table 2
Default and modified values of $C_{\varepsilon 2}$ and C_γ.

Run	$C_{\varepsilon 2}$	$C\gamma$
Default values	1.9	2.13
Modified EDC	1.9	5
Modified RKE	2.1	2.13
Modified EDC and RKE	2.1	5

Calculations carried out using modified values of $C_{\varepsilon 2}$ constant of the turbulence model and/or C_γ constant of the EDC model were carried out, as summarized in Table 2. The results obtained are shown in Fig. 10. The influence of the modification of C_γ is not as important as in run 1, yielding only a slight improvement in the temperature profile at $x = 150$ mm, and in the CO_2 profile at $x = 70$ mm. The modification of $C_{\varepsilon 2}$ is mainly visible at $x = 150$ mm, resulting in temperature and CO_2 molar fraction profiles in much closer agreement with the experimental ones, despite the underprediction of the temperature in the vicinity of the centreline. The best results are achieved when both constants are modified. However, the remark of Section 4.5 concerning the lack of theoretical reason to justify the change of the constants still holds.

At present, it is unclear why the models do not predict satisfactorily the combustion process in the vicinity of the burner. Further research is needed to clarify this issue, but it is tempting to speculate that large eddy simulation might be needed to describe the mixing and reaction process, and yield satisfactory predictions for the problem under investigation.

5. Conclusion

Numerical simulations of a laboratory reverse flow combustor burning natural gas have been reported for two operating conditions. The simulations were carried out using the realizable k–ε turbulence model and two different combustion models, namely the EDC and the C-PDF. The DRM19 chemical mechanism for natural gas, which is a reduced version of the GRI-Mech 1.2 mechanism, was employed. It was shown that the predictions can be considered grid independent and that an increase of the number of stochastic particles in the C-PDF

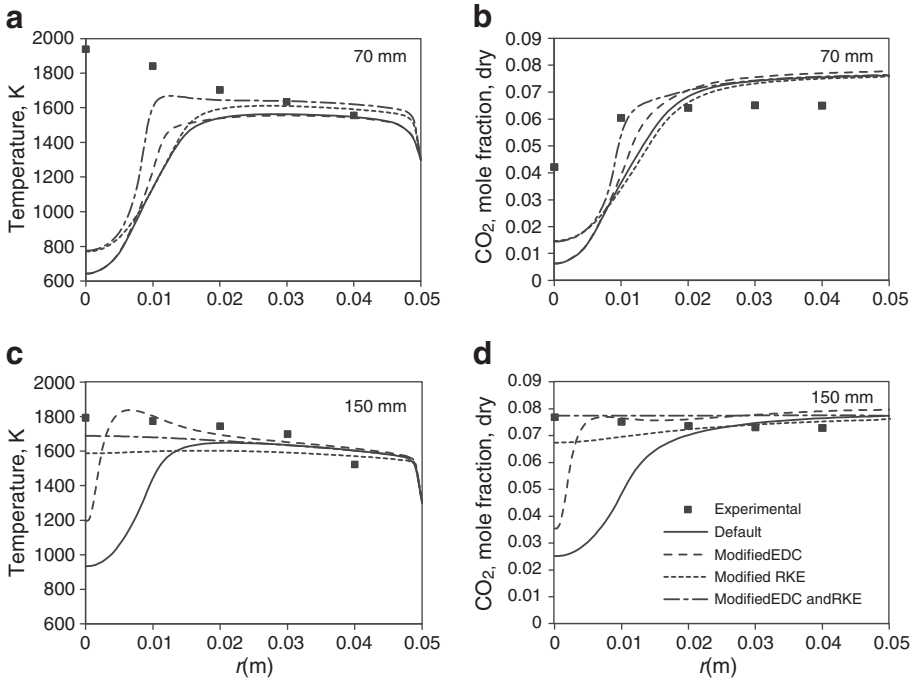

Fig. 8. Influence of the standard and modified constants of the turbulence and combustion models on the predictions for run 1.

has only a marginal influence on the results. The two combustion models yield similar results, and predict a delayed combustion process for both operating conditions. The temperature and the molar fraction of CO_2 are underestimated, while the O_2 molar fraction is overpredicted, in the region downstream of the burner extending up to about one-half of the length of the combustor. Elsewhere, a good agreement between the predictions and measurements of the temperature and molar fraction of the major species was found.

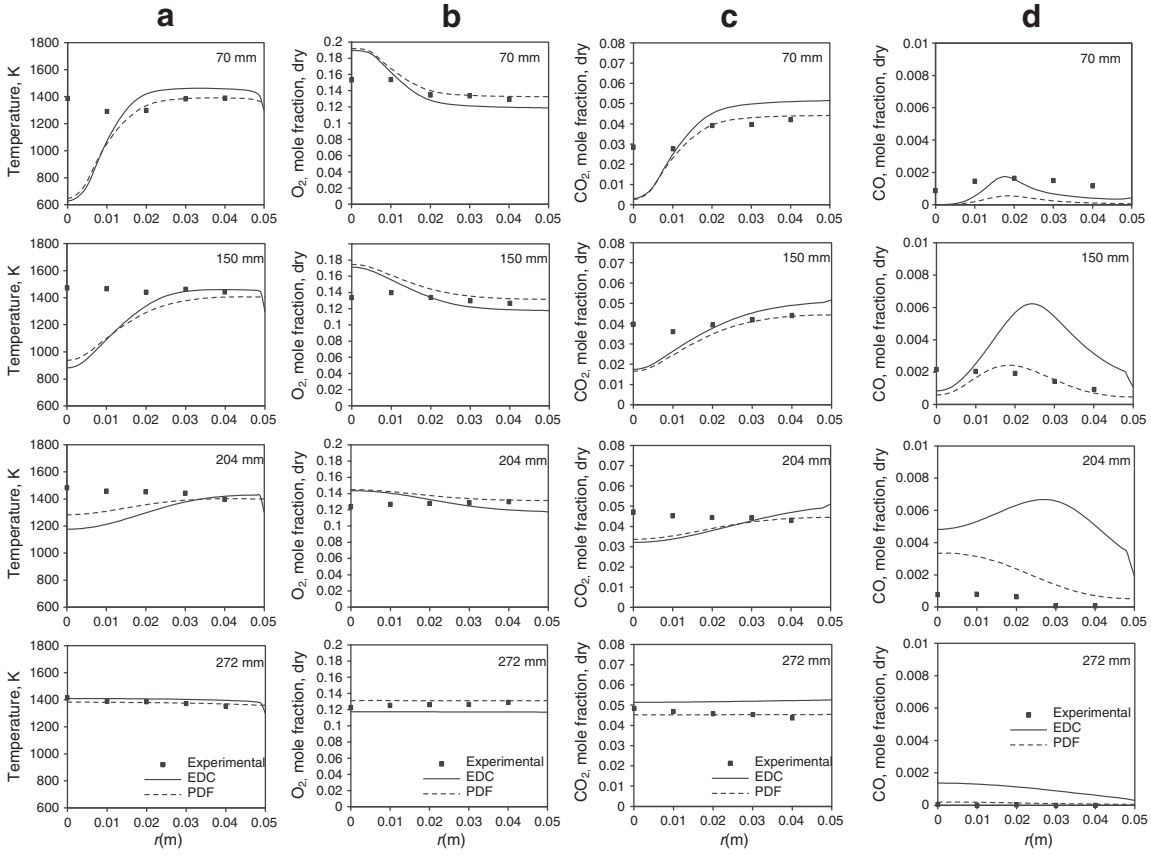

Fig. 9. Radial profiles of predicted temperature, O_2, CO_2 and CO dry mole fractions for run 2.

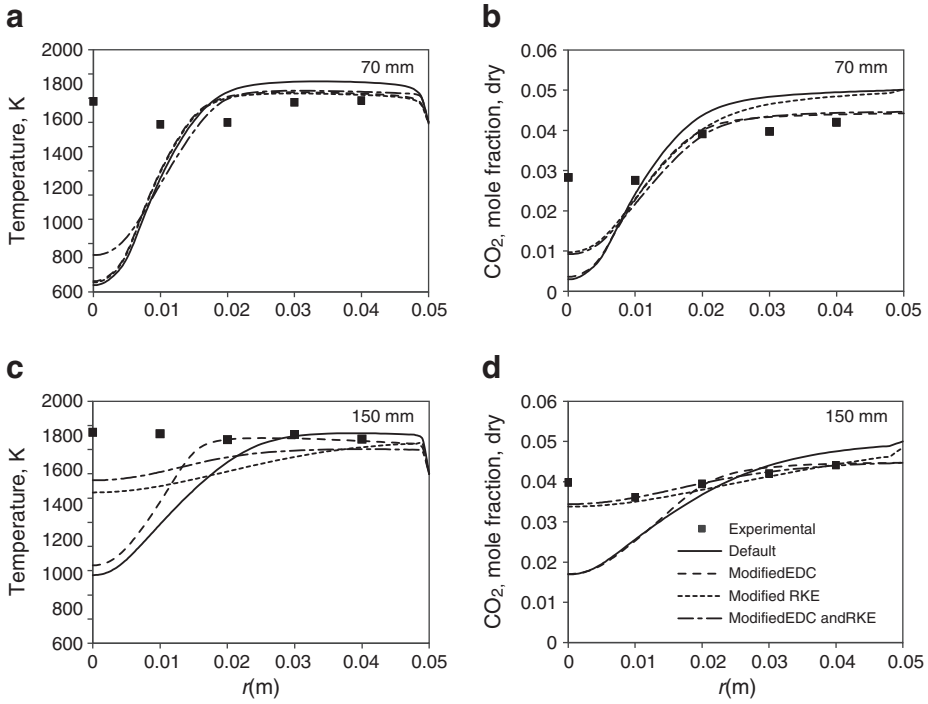

Fig. 10. Influence of the standard and modified constants of the turbulence and combustion models on the predictions for run 2.

Additional calculations using other first and second order closure turbulence models did not show any significant improvements. The results obtained using GRI-Mech 1.2 and DRM19 are quite close to each other, while a global model does not perform so well. It was further shown that the predictions may be improved by changing a constant of the turbulence model and/or the EDC volume fraction constant, but there is no theoretical reason to support the quantitative changes on a general basis. The ultimate reason for the failure of the models to reproduce the experimentally observed fast ignition and combustion close to the burner is unclear. It is speculated that a large eddy simulation model might be needed to describe the mixing and reaction processes in the near burner region, and might overcome the observed shortcomings of the present simulations.

Acknowledgements

This work was developed within the framework of project PTDC/EME-MFE/102997/2008, which is financially supported by Fundação para a Ciência e a Tecnologia (FCT). André Duarte is pleased to acknowledge UNL-FCT for the provision of a scholarship.

References

[1] J.A. Wünning, J.G. Wünning, Flameless oxidation to reduce thermal NO-formation, Progress in Energy and Combustion Science 23 (1997) 81–94.
[2] H. Tsuji, A.K. Gupta, T. Hasegawa, M. Katsuki, K. Kishimoto, M. Morita, High temperature air combustion: from energy conservation to pollution reduction, CRC Press, Boca Raton, 2003.
[3] J. Zeldovich, The oxidation of nitrogen in combustion and explosions, Acta Physicochimica URSS 21 (1946) 577–628.
[4] J. Wünning, Flameless Oxidation, In: 6th HiTACG Symposium — 2005, Essen-Germany, 17th–19th October 2005, 2005.
[5] M. Flamme, New combustion systems for gas turbines (NGT), Applied Thermal Engineering 24 (2004) 1551–1559.
[6] Y.D. Wang, Y. Huang, D. McIlveen-Wright, J. McMullan, N. Hewitt, P. Eames, S. Rezvani, A techno-economic analysis of the application of continuous staged-combustion and flameless oxidation to the combustor design in gas turbines, Fuel Processing Technology 87 (2006) 727–736.
[7] I. Nakamachi, K. Yasuzawa, T. Miyahata, Apparatus or method for carrying out combustion in a furnace, US Patent No.4, 945, 841, 1990.
[8] R. Weber, J. Dugué, A. Sayre, H. Horsmann, Scaling characteristics of the aerodynamics and low NO_x properties of industrial natural gas burners, In: IFRF Rep. No. F/40/y/9, The Scaling 400 Study, Part II: the 12 MW test results, 1993.
[9] D. Tabacco, C. Innarella, C. Bruno, Theoretical and numerical investigation on flameless combustion, Combustion Science and Technology 174 (2002) 1–35.
[10] H. Schütz, R. Lückerath, T. Kretschmer, B. Noll, M. Aigner, Analysis of the pollutant formation in the FLOX® combustion, Journal of Engineering for Gas Turbines and Power 130 (2008) 011503.
[11] D. Lupant, B. Pesenti, P. Evrard, P. Lybaert, Numerical and experimental characterization of a self-regenerative flameless oxidation burner operation in a pilot-scale furnace, Combustion Science and Technology 179 (2007) 437–453.
[12] C. Galletti, A. Parente, L. Tognotti, Numerical and experimental investigation of a mild combustion burner, Combustion and Flame 151 (2007) 649–664.
[13] S. Kumar, P.J. Paul, H.S. Mukunda, Studies on a new high-intensity low-emission burner, Proceedings of the Combustion Institute 29 (2002) 1131–1137.
[14] T. Plessing, N. Peters, J.G. Wünning, Laseroptical investigation of highly preheated combustion with strong exhaust gas recirculation, Proceedings of the Combustion Institute 27 (1998) 3197–3204.
[15] B.I. Özdemir, N. Peters, Characteristics of the reaction zone in a combustor operating at mild combustion, Experiments in Fluids 30 (2001) 683–695.
[16] P.J. Coelho, N. Peters, Numerical simulation of a mild combustion burner, Combustion and Flame 124 (2001) 503–518.
[17] B.B. Dally, E. Riesmeier, N. Peters, Effect of fuel mixture on moderate and intense low oxygen dilution combustion, Combustion and Flame 137 (2004) 418–431.
[18] G.G. Szegö, B.B. Dally, G.J. Nathan, Scaling of NO_x emissions from a laboratory-scale mild combustion furnace, Combustion and Flame 154 (2008) 281–295.
[19] G.G. Szegö, B.B. Dally, G.J. Nathan, Operational characteristics of a parallel jet MILD combustion burner system, Combustion and Flame 2 (2009) 429–438.
[20] E.E. Khalil, Assessment of numerical computation of flow properties in an axi-symmetric reversed flow furnace, Applied Mathematical Modelling 3 (1979) 25–31.
[21] M.S. Mansour, R.W. Bilger, R.W. Dibble, Raman/Rayleigh and mie-scattering measurements in a reverse flow reactor close to extinction, Proceedings of the Combustion Institute 22 (1989) 711–719.
[22] M.K. Bobba, P. Gopalakrishnan, K. Periagaram, J.M. Seitzman, Flame structure and stabilization mechanisms in a stagnation-point reverse-flow combustor, Journal of Engineering for Gas Turbines and Power 130 (2008) 031505.
[23] P. Gopalakrishnan, M.K. Bobba, J.M. Seitzman, Controlling mechanisms for low NOx emissions in a non-premixed stagnation point reverse flow combustor, Proceedings of the Combustion Institute 31 (2007) 3401–3408.
[24] S. Undapalli, S. Srinivasan, S. Menon, LES of premixed and non-premixed combustion in a stagnation point reverse flow combustor, Proceedings of the Combustion Institute 32 (2009) 1537–1544.
[25] M. Castela, A.S. Veríssimo, A.M.A. Rocha, M. Costa, Experimental study of the combustion regimes occurring in a laboratory combustor, Combustion Science and Technology 184 (2012) 243–258.
[26] S. Orsino, R. Weber, U. Bollettini, Numerical simulation of combustion of natural gas with high-temperature air, Combustion Science and Technology 171 (2001) 1–34.

[27] M. Mancini, P. Schwoppe, R. Weber, S. Orsino, On mathematical modelling of flameless combustion, Combustion and Flame 150 (2007) 54–59.
[28] B. Danon, W. de Jong, D.J.E.M. Roekaerts, Experimental and numerical investigation of a flox combustor firing low calorific value gases, Combustion Science and Technology 182 (2010) 1261–1278.
[29] F.C. Christo, B.B. Dally, Modeling turbulent reacting jets issuing into a hot and diluted coflow, Combustion and Flame 142 (2005) 117–129.
[30] B.F. Magnussen, On the structure of turbulence and a generalized eddy dissipation concept for chemical reaction in turbulent flow, In: 19th AIAA Aerospace Science Meeting, AIAA-2006-0962, 1981.
[31] S. Kumar, P.J. Paul, H.S. Mukunda, Prediction of flame liftoff height of diffusion/partially premixed jet flames and modeling of mild combustion burners, Combustion Science and Technology 179 (2007) 2219–2253.
[32] J.P. Kim, U. Schnell, G. Scheffknecht, Comparison of different global reaction mechanisms for mild combustion of natural gas, Combustion Science and Technology 180 (2008) 565–592.
[33] A. Parente, C. Galletti, L. Tognotti, Effect of the combustion model and kinetic mechanism on the MILD combustion in an industrial burner fed with hydrogen enriched fuels, International Journal of Hydrogen Energy 33 (2008) 7553–7564.
[34] N. Krishnamurthy, P.J. Paul, W. Blasiak, Studies on low-intensity oxy-fuel burner, Proceedings of the Combustion Institute 32 (2009) 3139–3146.
[35] J. Mi, P. Li, B.B. Dally, R.A. Craig, Importance of initial momentum rate and air–fuel premixing on moderate or intense low oxygen dilution (mild) combustion in a recuperative furnace, Energy and Fuels 23 (2009) 5349–5356.
[36] A. Parente, C. Galletti, L. Tognotti, A simplified approach for predicting NO formation in MILD combustion of CH4–H2 mixtures, Proceedings of the Combustion Institute 33 (2011) 3343–3350.
[37] B. Danon, E.S. Cho, W. de Jong, D.J.E.M. Roekaerts, Numerical investigation of burner positioning effects in a multi-burner flameless combustion furnace, Applied Thermal Engineering 31 (2011) 3885–3896.
[38] A. Frassoldati, P. Sharma, A. Cuoci, T. Faravelli, E. Ranzi, Kinetic and fluid dynamics modeling of methane/hydrogen jet flames in diluted coflow, Applied Thermal Engineering 30 (2010) 376–383.
[39] A. Mardani, S. Tabejamaat, M. Ghamari, Numerical study of influence of molecular diffusion in the mild combustion regime, Combustion Theory and Modelling 14 (2010) 747–774.
[40] A. Mardani, S. Tabejamaat, Effect of hydrogen on hydrogen–methane turbulent non-premixed flame under MILD condition, International Journal of Hydrogen Energy 35 (2010) 11324–11331.
[41] J. Aminian, C. Galletti, S. Shahhosseini, L. Tognotti, Key modeling issues in prediction of minor species in diluted-preheated combustion conditions, Applied Thermal Engineering 31 (2011) 3287–3300.
[42] A. De, E. Oldenhof, P. Sathiah, D. Roekaerts, Numerical simulation of delft-jet-in-hot-coflow (DJHC) flames using the eddy dissipation concept model for turbulence–chemistry interaction, Flow, Turbulence, and Combustion 87 (2011) 537–567.
[43] A. Mardani, S. Tabejamaat, M.B. Mohammadi, Numerical study of the effect of turbulence on rate of reactions in the MILD combustion regime, Combustion Theory and Modelling 15 (2011) 753–772.
[44] J. Aminian, C. Galletti, S. Shahhosseini, L. Tognotti, Numerical Investigation of a MILD Combustion Burner: Analysis of Mixing Field, Chemical Kinetics and Turbulence-Chemistry Interaction, Flow, Turbulence, and Combustion. http://dx.doi.org/10.1007/s10494-012-9386-z.
[45] S.B. Pope, PDF methods for turbulent reactive flows, Progress in Energy and Combustion Science 11 (1985) 119–192.
[46] F.C. Christo, B.B. Dally, Application of Transport PDF Approach for Modelling MILD Combustion, In: 15th Australasian Fluid Mechanics Conference, The University of Sydney, Sydney, Australia 13–17 December 2004, 2004.
[47] T.H. Shih, W.W. Liou, A. Shabbir, J. Zhu, A new k–ε Eddy-Viscosity Model for High Reynolds number turbulent flows — model development and validation, Computers and Fluids 24 (1995) 227–238.
[48] B.F. Magnussen, B.H. Hjertager, On mathematical modeling of turbulent combustion with special emphasis on soot formation and combustion, Proceedings of the Combustion Institute 16 (1977) 719–729.
[49] S. Subramaniam, S.B. Pope, A mixing model for turbulent reactive flows based on euclidean minimum spanning trees, Combustion and Flame 115 (1998) 487–514.
[50] A. Kazakov, M. Frenklach, http://www.me.berkeley.edu/drm/ [cited February 29 2012].
[51] M. Frenklach, H. Wang, C.-L. Yu, M. Goldenberg, C.T. Bowman, R.K. Hanson, D.F. Davidson, E.J. Chang, G.P. Smith, D.M. Golden, W.C. Gardiner, V. Lissianski, http://www.me.berkeley.edu/gri_mech/ [cited February 29 2012].
[52] C.K. Westbrook, F.L. Dryer, Simplified reaction mechanisms for the oxidation of hydrocarbon fuels in flames, Combustion Science and Technology 27 (1981) 31–43.
[53] S.B. Pope, Computationally efficient implementation of combustion chemistry using in situ adaptive tabulation, Combustion Theory and Modelling 1 (1997) 41–63.
[54] H.K. Versteeg, W. Malalasekera, An Introduction to Computational Fluid Dynamics, second ed. Pearson Education Limited, Essex, England, 2007.
[55] M. Rehm, P. Seifert, B. Meyer, Theoretical and numerical investigation on the EDC-Model for turbulence-chemistry interaction at gasification conditions, Computers and Chemical Engineering 33 (2009) 402–407.